Optics Letters

Single-pulse, reference-free, spatiotemporal characterization of ultrafast laser pulse beams via broadband ptychography

David Goldberger,* Jonathan Barolak, David Schmidt, Bojana Ivanic, Claudia A. M. Schrama, Christopher Car, Rhiannon Larsen, Charles G. Durfee, and Daniel E. Adams

Department of Physics, Colorado School of Mines, 1523 Illinois Street, Golden, Colorado 80401, USA
**DavidLGoldberger@gmail.com*

Received 4 May 2023; accepted 24 May 2023; posted 31 May 2023; published 21 June 2023

Ultrafast laser pulse beams are four-dimensional, space–time phenomena that can exhibit complicated, coupled spatial and temporal profiles. Tailoring the spatiotemporal profile of an ultrafast pulse beam is necessary to optimize the focused intensity and to engineer exotic spatiotemporally shaped pulse beams. Here we demonstrate a single-pulse, reference-free spatiotemporal characterization technique based on two colocated synchronized measurements: (1) broadband single-shot ptychography and (2) single-shot frequency resolved optical gating. We apply the technique to measure the nonlinear propagation of an ultrafast pulse beam through a fused silica window. Our spatiotemporal characterization method represents a major contribution to the growing field of spatiotemporally engineered ultrafast laser pulse beams.

https://doi.org/10.1364/OL.493234

High-intensity, ultrafast pulse beams of light are used in a variety of scientific and industrial applications, including particle acceleration, secondary source generation, micromachining, and more [1]. In many applications, ultrafast pulse beams are used to optimize the intensity of light focused onto a target. Recently, more exotic spatiotemporally engineered ultrafast pulse beams have been demonstrated as well. These include propagation-invariant space-time wave packets [2], spatiotemporal optical vortices [3], and simultaneous spatial and temporal focusing [4]. As shown by these examples, engineering the spatiotemporal profile of an ultrafast pulse beam provides new dimensions of control that we are just beginning to explore [5]. Spatiotemporal characterization is critical for controlling spatiotemporal profiles to engineer exotic shapes and to optimize the focused intensity. Single-shot measurement is crucial for characterizing the pulse beam used for single-shot experiments, analyzing the stability of multi-pulse experiments, and providing rapid feedback for dynamically optimized shaping.

Recent review articles outline the multiple intersecting challenges involved in measuring the spatiotemporal profile of an ultrafast laser pulse beam [6,7]. In short, spatiotemporal coupling, present in nearly all ultrafast pulse beams, means that the field cannot be written in separable form, i.e., $E(x, y, z, t) \neq f(x, y, z)g(t)$. The inseparability of spatial and temporal electric field profiles necessitates measurement techniques that simultaneously measure in both domains. Many spatiotemporal measurement techniques require scanning part of the system, which precludes single-shot or single-pulse measurement [6,7]. In recent years, a number of techniques have been developed for single-shot, reference-free or self-referenced, full-field spatiotemporal characterization [8–10]. Here we present a precise method for single-shot, reference-free, full-field spatiotemporal characterization and demonstrate the utility of our method by measuring the nonlinear propagation of a single, ultrafast pulse beam through a fused silica window.

Our spatiotemporal measurement device is based on broadband single-shot ptychography (BBSSP) [11,12]. Single-shot ptychographic microscopes have received attention in recent years for their ability to image multiple noninterfering channels in both amplitude and phase [13–15]. BBSSP measures the spectrally resolved spatial amplitude and phase of the electric field, $\tilde{E}(x, y, z_0, \omega)$, at the object plane in the BBSSP microscope, $z = z_0$. Since the complex spatial profile is measured for each spectral component, the field can be propagated axially to generate the four-dimensional spatiospectral field, $\tilde{E}(x, y, z, \omega)$. BBSSP does not measure the spectral phase of the electric field, so an additional measurement of the spectral phase at one known location, $\varphi(x_0, y_0, z_r, \omega)$, is required before the spatiospectral electric field can be Fourier transformed to get the spatiotemporal field $E(x, y, z, t)$. Here, z_r is some known reference plane. We use reflective, single-shot, second harmonic generation, frequency resolved optical gating (SSFROG) for the spectral phase measurement because it is robust and energy efficient [16,17].

A schematic of our measurement system and the spatiotemporal profile of a single pulse beam are shown in Fig. 1. In our system, an ultrafast pulse beam is produced by a Ti:Sapphire amplifier system (Spectra Physics Solstice Ace). The pulse beam is split into two copies by a 99/1% amplitude beam splitter (LAYERTEC 108325). The high-energy portion of the beam is reflected to the SSFROG measurement arm, while the low-energy portion goes to the BBSSP measurement arm. The

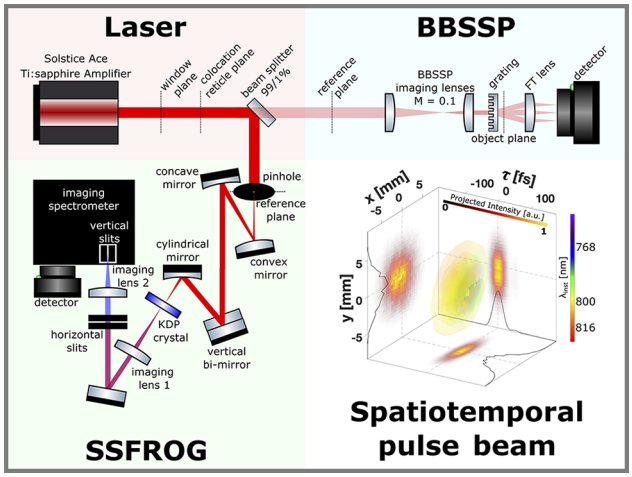

Fig. 1. Schematic of single-pulse, reference-free, spatiotemporal measurement system and the measured spatiotemporal profile of a single pulse. The measurement system is broken into three sections: the laser, the BBSSP system, and the SSFROG system. The spatiotemporal profile is displayed as described in section S2 of the SD.

BBSSP microscope is as described in [12], the SSFROG is as described in [17], and further details can be found in section S1 of the Supplemental document (SD).

Colocation is a subtle and often overlooked aspect of combining spatiospectral and temporal measurements. Specifically, temporal measurement must be made at a known spatial location relative to spatiospectral measurement. Figure 2 shows simulations that demonstrate how correct versus incorrect colocation leads to significantly different spatiotemporal profiles. To create a pulse beam with an interesting spatiotemporal profile, we simulated the nonlinear propagation of a transform-limited, 4.5-mm diameter pulse beam through a 3-mm-thick piece of fused silica. The simulation was performed with the nonlinear propagation code described in the SD. The "correctly colocated" pulses are simply the results of these simulations plotted in spacetime. To simulate the effect of incorrect colocation, we replace the spectral phase at the center spatial location of the pulse beam with the spectral phase from a position approximately 2.5 mm (10 pixels) off center. These positions are shown by the green dot and red x in the xy profiles on the spatiotemporal plots, respectively. Here we chose a large misalignment to emphasize the effect of incorrect colocation. We performed this analysis for two pulse beams with different spectra; one centered at 1500 nm and one at 800 nm to examine the difference between anomalous and normal dispersion in fused silica. Both pulses shared the same fractional bandwidth, $\frac{\Delta\lambda}{\lambda_0} = 6.25\%$, where $\Delta\lambda$ is the spectral full width at half maximum and λ_0 is the central wavelength.

In our measurement system, the BBSSP arm provides the complex spatiospectral electric field at the object plane in the microscope, which (assuming ideal imaging) is a demagnified copy of the field at the reference plane, $\tilde{E}(x, y, z_r, \omega)$. The SSFROG arm provides the complex spectral profile at the location of the pinhole, $\tilde{E}(x_0, y_0, z_r, \omega)$. Placing the pinhole and the image plane of the BBSSP system the same distance away from the beam splitter ensures that the two measurements are colocated axially (at z_r), but colocating them transverse to the beam propagation requires additional calibration.

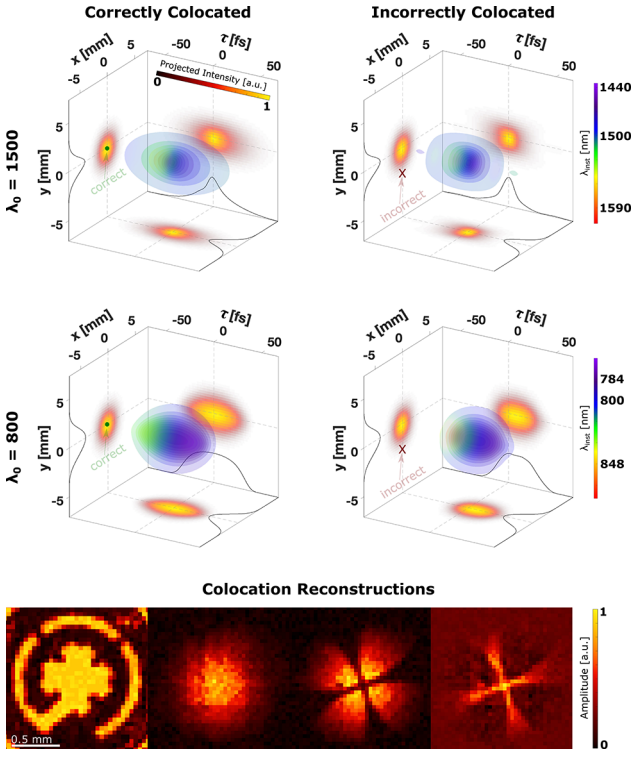

Fig. 2. Simulations showing the necessity of accurately colocating spatiospectral and temporal measurements and reconstructions from our colocation calibration method. The spatiotemporal profiles are displayed as described in section S2 of the SD, and the markers on the xy profiles indicate where the spectral phase was measured. From left to right, the bottom row shows the reconstructed object, probe intensity from the dataset without the reticle, the reconstructed probe from the dataset with the reticle, and the difference between the probe reconstructions.

For transverse colocation, we place an interference filter and a reticle with a 350-μm central cross just upstream of the beam splitter. We define the resulting illumination at the reference plane $E_{ref}(x, y, z_r)$, which is the shadow of the reticle. In the SSFROG arm, we image $E_{ref}(x, y, z_r)$ to a camera. We place the pinhole on a translation stage and translate it until it overlaps with the shadow of the central cross from the reticle. In the BBSSP arm, we collect single-wavelength data with and without the reticle in place, without moving the object between the data collections. We reconstruct the object and probe from the dataset without the reticle, then we use the object from that reconstruction as a constraint to reconstruct the dataset with the reticle. Since the object did not move between the data collections, using the previously reconstructed object as a constraint in the second reconstruction ensures that the probe reconstructions with and without the reticle share the same field of view. The difference between the probe reconstructions yields unambiguous determination of the location of the central cross shadow relative to the reconstructed probe field of view. As long as the object in the BBSSP system does not move and the original object reconstruction is used as a constraint, that location does not change from reconstruction to reconstruction. The object and probe reconstructions with and without the reticle as well as the difference between the probe reconstructions are shown in the bottom row of Fig. 2. The ground truth for the object reconstruction is shown in [12]. The colocation

calibration only needs to be performed once before single-pulse data collection and it is valid as long as the relative position of all components downstream of the beam splitter remains constant.

The pulse beam measurement can be broken into two steps: data collection and reconstruction. An important part of single-pulse measurement is synchronizing the BBSSP and SSFROG detectors so that they measure the same pulse beam. We accomplish this by using the same detector models in each system (Thorlabs 8051M) and sending the same trigger signal from a digital delay generator (DDG) to each detector. The DDG trigger signal initializes the exposure on each detector and we set the exposure times to 9 ms, which ensures that only illumination from a single pulse can be captured since the laser repetition rate is 100 Hz. All of the results that we show are from single pulses, no stitching of multiple exposures to generate high dynamic range images or collection of additional data to implement modulus enforcement on the probe is involved [12]. To reconstruct the spatiotemporal profile of a single pulse, the BBSSP and SSFROG data are first reconstructed independently. The BBSSP reconstructions are performed with the PIM-RAAR algorithm adapted for BBSSP [11,12]. The SSFROG reconstructions are performed with the SVD FROG algorithm [18,19]. Reconstruction details are in section S1 of the SD.

As a result of colocation, the BBSSP and SSFROG reconstructions can be combined accurately. The complex spatiospectral field reconstructed from BBSSP, $\tilde{E}_B$, is combined with the spectral phase reconstructed by SSFROG, φ_F, at the position identified in the colocation calibration by replacing the random spectral phase from BBSSP, φ_B, with φ_F, i.e., $\tilde{E}(x, y, z_r, \omega) = \tilde{E}_B(x, y, z_r, \omega)e^{i\varphi_F(x_0,y_0,z_r,\omega)-i\varphi_B(x_0,y_0,z_r,\omega)}$. We zero-pad the spectral dimension before Fourier transforming to the spatiotemporal profile, $E(x, y, z_r, t)$, with temporal pixel size of approximately 2.8 fs. The spatiospectral electric field can also be propagated to any other axial plane z before Fourier transforming to get the spatiotemporal electric field.

To demonstrate the capabilities of our single-pulse spatiotemporal measurement device, we characterized ultrafast pulse beams from a Ti:Sapphire amplifier system (Spectra Physics Solstice Ace). For our experiments, the amplifier ran at a repetition rate of 100 Hz and produced roughly 10-mm diameter beams of approximately 6-mJ pulse energy, as measured at the output of the amplifier. We took advantage of the ability to change the grating separation in the compressor of the amplifier to control the spectral phase and temporal duration of the pulses we characterized. We did not rigorously identify optimal compression, but we characterized a pulse beam at near optimal compression, as shown in Fig. 1, and found that the pulse duration was approximately 40 fs.

To highlight the single-pulse capabilities of our system and the stability of our amplifier, we characterized six individual pulses with the amplifier at the same conditions. Three of the pulses were measured on the first day of the experiment and three more were measured the following day. Each set of three pulses was measured over the course of a few minutes—not sequentially. For this experiment, the grating separation in the amplifier was intentionally moved away from optimal compression to generate pulses with noticeable temporal chirp. Figures 3 and S1 show the results of this experiment. To confirm the accuracy of our colocation method, we compare the average full width at half maximum of the spectrum from BBSSP at the colocation point to that retrieved from SSFROG and find good

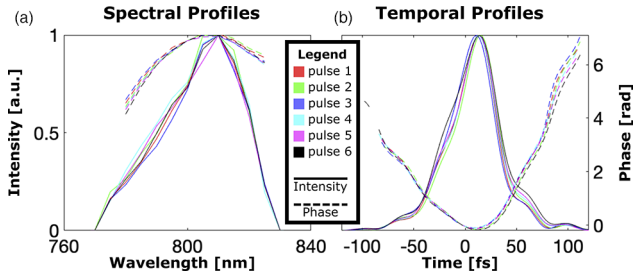

Fig. 3. Results from the experiment to confirm the pulse-to-pulse stability of our amplifier. Six different pulses were characterized. The (a) complex spectral and (b) temporal profiles of the six pulses are shown, as measured at the colocation position.

agreement ($\text{FWHM}_F = 26.0 \pm 1.5$, $\text{FWHM}_B = 26.7 \pm 2.6$). The spatiotemporal profiles of all six pulse beams agree well. The mean standard deviation per pixel is 1.2%, which gives confidence in the stability of the amplifier and measurement system. If we assume that the amplifier produces identical pulses, the instability we observe indicates the precision of our measurement system. However, it is also possible that the instability is caused by pulse-to-pulse fluctuations from the amplifier. While we did not determine its exact source here, the observed instability demonstrated the power of the single-pulse measurement capabilities of our technique. Measurement of pulse-to-pulse fluctuations could provide valuable insights for higher-energy, lower-repetition-rate ultrafast laser systems.

To demonstrate the utility and confirm the accuracy of our measurement technique, we measured the nonlinear propagation of a single ultrafast pulse beam through a glass window. We placed a roughly 4-mm-thick fused silica window 5 cm upstream of the beam splitter at the "window plane" as shown in Fig. 1. We collected single-pulse data with and without the window in the system, and we measured the pulse energy just upstream of the window as 4.75 mJ. The amplifier was set to the same conditions as for the stability experiment, so the pulse beam we characterized without the window in the system (Fig. S2, left) looks similar to those shown in Fig. S1. The pulse we characterized with the glass in the system (Fig. S2, middle) is significantly different. Part of the beam is blocked by a fiducial placed on the back of the window to help identify that axial plane, and the spatiotemporal profile is altered due to the nonlinear propagation of the pulse beam through the window.

Assuming pulse-to-pulse fluctuations are negligible, since the amplifier's setting did not change between measurements, any differences between the pulse beams we characterized with and without the window in the system are due to the nonlinear propagation of the pulse beam through the window. Nonlinear pulse beam propagation is the subject of ongoing research, and models to simulate it are still evolving [20]. For our experiment, we wrote a split-step, four-dimensional, nonlinear propagation code that accounts for frequency dependent diffraction, dispersion, Kerr nonlinearity, and the delayed Raman response. Further details on the simulation code and parameters we used for simulation can be found in section 3 of the SD. We backpropagate the spatiotemporal profile of the pulse beam measured without glass to the front of the glass window and use the result, shown in Fig. S2 left, as the input to the simulation. The simulation yields the spatiotemporal profile at the back surface of the glass window which is shown in Fig. S2 right, and compares well with the spatiotemporal profile of the pulse beam we characterized with the

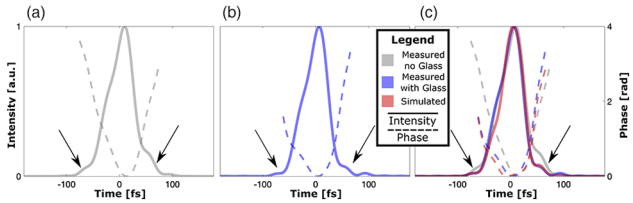

Fig. 4. Comparison of measured and simulated nonlinear pulse beam propagation through fused silica window. (a) Temporal profile (plotted through the maximum intensity spatial pixel) of the pulse beam we characterized without the window in the system, backpropagated to the front plane of the window, which is the input to the simulation. (b) The same as panel (a), but with the window in the system and backpropagated to the back plane of the window. (c) Both experimental and the simulated temporal profiles shown for comparison. The simulated and experimental result compare well, which confirms the accuracy and demonstrates the utility of our measurement technique.

window in the system backpropagated to the same plane, shown in Fig. S2 middle. Apart from the small missing spatial portion of the beam that was blocked by the fiducial, the spatiotemporal profiles look almost identical. The temporal profiles displayed in Fig. 4 show that the simulated nonlinear pulse propagation agrees with our measurement. In both cases, we observe slight pulse compression which is expected due to the negative spectral chirp of the input pulse. This agreement confirms the accuracy of our measurement technique. Since the nonlinear pulse beam propagation simulation uses the full spatiotemporal profile of the pulse beam, if either the spatial or temporal profiles we measured were incorrect, the simulation would not have generated the same spatiotemporal profile as we measured. In addition to validating our measurement system, this experiment gives an example of how single-pulse spatiotemporal measurements can be used to refine physical models, including nonlinear pulse beam propagation. As higher-intensity pulses are generated, the models needed to understand them become more complicate, and metrologies like ours will be critical to informing these models.

We have introduced a single-pulse, reference-free, spatiotemporal measurement system based on synchronized, colocated, BBSSP and SSFROG. The spatiospectral electric field characterized by BBSSP is combined with the spectral phase measured by SSFROG to give the full, complex, four-dimensional spatiotemporal electric field, $E(x, y, z, t)$, of a single pulse. We described our colocation calibration technique and other subtleties involved in correctly measuring spatiotemporal profiles. In our first experiment, we showed that our amplifier was stable and in our second experiment, we compared measured and simulated nonlinear propagation of a pulse beam through a glass window. Our second experiment confirms the accuracy of our measurement system and gives one example of how such measurements can be used to inform physical models. Our single-pulse, reference-free, spatiotemporal measurement system represents a significant contribution to the field of spatiotemporally engineered ultrafast lasers. It can be used to mitigate spatiotemporal aberrations to optimize the focused intensity. Additionally, we expect our work to gain relevance as researchers explore the new dimensions of control that spatiotemporally engineered pulses yield.

Funding. Air Force Office of Scientific Research (FA9550-22-1-0495); National Science Foundation (2206807).

Disclosures. The authors declare no conflicts of interest.

Data availability. Data underlying the results presented in this paper are not publicly available at this time but may be obtained from the authors upon reasonable request.

Supplemental document. See Supplement 1 for supporting content.

REFERENCES

1. C. N. Danson, C. Haefner, and J. Bromage, *et al.*, High Power Laser Sci. Eng. **7**, e54 (2019).
2. A. M. Motz, M. Yessenov, and A. F. Abouraddy, Phys. Rev. Appl. **15**, 024067 (2021).
3. N. Jhajj, I. Larkin, E. W. Rosenthal, S. Zahedpour, J. K. Wahlstrand, and H. M. Milchberg, Phys. Rev. X **6**, 031037 (2016).
4. E. Block, M. Greco, D. Vitek, O. Masihzadeh, D. A. Ammar, M. Y. Kahook, N. Mandava, C. Durfee, and J. Squier, Biomed. Opt. Express **4**, 831 (2013).
5. C. He, Y. Shen, and A. Forbes, Light: Sci. Appl. **11**, 205 (2022).
6. C. Dorrer, IEEE J. Sel. Top. Quantum Electron. **25**, 3100216 (2019).
7. S. W. Jolly, O. Gobert, and F. Quéré, J. Opt. **22**, 103501 (2020).
8. Y. G. Kim, J. I. Kim, J. W. Yoon, J. H. Sung, S. K. Lee, and C. H. Nam, Opt. Express **29**, 19506 (2021).
9. H. Tang, T. Men, X. Liu, Y. Hu, J. Su, Y. Zuo, P. Li, J. Liang, M. C. Downer, and Z. Li, Light: Sci. Appl. **11**, 244 (2022).
10. Y. Xu, Y. Yi, P. Zhu, X. Pan, Q. Zhang, L. Pan, F. Ding, D. Zhang, X. Liang, M. Sun, A. Guo, X. Zhang, H. Tao, Z. Guang, C. Liu, X. Xie, J. Zhu, and R. Trebino, Opt. Lett. **47**, 5664 (2022).
11. D. Goldberger, D. Schmidt, J. Barolak, B. Ivanic, C. G. Durfee, and D. E. Adams, Opt. Express **29**, 32474 (2021).
12. D. Goldberger, J. Barolak, C. S. Bevis, B. Ivanic, D. Schmidt, Y. Lei, P. Kazansky, G. F. Mancini, C. G. Durfee, and D. E. Adams, Optica **9**, 894 (2022).
13. B. K. Chen, P. Sidorenko, O. Lahav, O. Peleg, and O. Cohen, Opt. Lett. **43**, 5379 (2018).
14. D. Goldberger, J. Barolak, C. G. Durfee, and D. E. Adams, Opt. Express **28**, 18887 (2020).
15. J. Barolak, D. Goldberger, J. Squier, Y. Bellouard, C. Durfee, and D. Adams, Ultramicroscopy **233**, 113418 (2022).
16. D. J. Kane and R. Trebino, Opt. Lett. **18**, 823 (1993).
17. S. Akturk, C. D'Amico, and A. Mysyrowicz, J. Opt. Soc. Am. B **25**, A63 (2008).
18. D. Kane, IEEE J. Sel. Top. Quantum Electron. **4**, 278 (1998).
19. A. Wyatt, "Frequency-resolved optical gating (FROG)," matlabcentral2008https://www.mathworks.com/matlabcentral/fileexchange/16235-frequency-resolved-optical-gating-frog.
20. F. Vidal, J. Phys. B: At., Mol. Opt. Phys. **53**, 055401 (2020).